Holocene evolution and signature of environmental change of the Burullus lagoon (Nile Delta) deciphered from a long sediment record

Matthieu Giaime, Alaa Salem, Yanna Wang, Xiaoshuang Zhao, Yan Liu, Jing Chen, Qianli Sun, A.M. Abu Shama, M.M. Elhossainy, Christophe Morhange, et al.

Holocene evolution and signature of environmental change of the Burullus lagoon (Nile Delta) deciphered from a long sediment record

Matthieu Giaime [a,b], Alaa Salem[c], Yanna Wang[d*], Xiaoshuang Zhao[d], Yan Liu[d], Jing Chen[d], Qianli Sun[d], Abu Shama A. M[c], M.M. Elhossainy[b], Christophe Morhange[e,f], Zhongyuan Chen[d*]

a) Department of Geography, Durham University, South Road, Durham, DH1 3LE, UK

b) Present address: Institut de Ciència i Tecnologia Ambientals (ICTA-UAB), Universitat Autònoma de Barcelona, 08193 Cerdanyola del Vallès, Barcelona, Spain

c) Kafrelsheikh University, Faculty of Science, Kafrelsheikh, Egypt

d) State Key laboratory for Estuarine and Coastal Research, East China Normal University, Shanghai 200062, China

e) Aix Marseille University, CNRS, IRD, INRAE, Coll France, CEREGE, Aix-en-Provence, 13090, France

f) EPHE, PSL, Les Patios Saint-Jacques, 4-14 rue Ferrus 75014 Paris

Corresponding author.

E-mail: z.chen@sklec.ecnu.edu.cn (z. chen)； ynwang@sklec.ecnu.edu.cn (YN Wang)

Abstract

This study presents high-resolution multi-proxy analyses of a well-dated sediment core (BR-1, 19.20 m long) retrieved from the Nile Delta, aiming to reconstruct the Holocene evolution of the Burullus lagoon. In particular, we focus on the morphodynamical processes, sediment provenances and related hydro-climatic changes. The Holocene strata of the lagoon coast comprise Early-Holocene marine transgressive facies and the Mid-Late Holocene retrogressive deltaic facies. Although BR-1 shows no river-channel facies, two peaks of magnetic susceptibility (MS) at ca. 8.0-7.0 ka (also associated with a high sedimentation rate of 50 mm/yr) and 3.5-2.0 ka evoke phases of greater morphodynamic influence of palaeo-Nile branches on the lagoon's development. Both dated peat layers (ca. 13 m and 8 m below MSL) and lagoon muds intercalated in BR-1, together with previously-dated peat strata were benchmarked relatively to MSL for the reconstruction of relative Holocene sea level in the study area. Our results show considerable land lowering on the Burullus coast indicated by a sea-level elevation, ca. 4-1 m lower than the one reconstructed along adjacent coastlines where less land subsidence occurred. The lagoon system began to form after ca. 6.0 ka in response to deceleration in sea-level rise and, being a shallower water body, both macrofauna (*Cerastoderma glaucum* etc.) and ostracods (*Cyprideis torosa*) of brackish-water nature emerged. In addition, geochemical data from BR-1 provide insights into environmental change in association with basin-wide hydro-climate fluctuations. Concomitant peaks in Fe/Al, Ti/Al and Cr/Al ratios (mafic origin), together with higher Zr/Al and Hf/Al ratios (felsic origin) before ca. 8.0 ka suggest sediment provenances derived from the White and the Blue Nile during the main African Humid Period (AHP). Since then, Ti/Al kept slightly ascending core-upwards with two pulses at 7.8-7.3 ka and 3.5-2.0 ka, which was asynchronous to Zr/Al and Hf/Al. This corroborates more sediments of basaltic origin transported to the delta coast after the main AHP due to southerly shift in the position of the ITCZ. The two periods of Ti/Al pulse are consistent with the MS peaks in BR-1, suggesting that palaeo-Nile branches remained active during 8.0-7.0 ka and 3.0-2.0 ka nearby.

Keywords: Sediment provenance; Diagnostic geochemical elements; Source to Sink; Sea-level rise, Sedimentation rate, Paleogeography

1. Introduction

Continental rivers and their mega-deltas constitute rich archives of Holocene environmental change and human activities (Törnqvist, 1994; Stanley and Warne, 1997; Krom, et al., 2002; Kennett and Kennett, 2006; Day et al., 2007; Chen et al., 2008; Marriner et al., 2013; Zuo et al., 2016). In recent decades, deltaic coastlines became highly vulnerable, primarily resulting from the rising sea level and the intensification of human activities both on delta plains and in watersheds, leading to a dramatic reduction in sediment supply to deltaic coasts (Syvitski et al., 2009; Renaud et al., 2013; Anthony et al., 2014; Brown and Nicholls, 2015; Tessler et al., 2016; Besset et al., 2019).

The Nile Delta is a subsiding sedimentary sink that hosts ca. 41% of Egypt's population and 60% of the country's food production (Hereher, 2010). Projected scenarios of relative sea-level rise for the coming decades have sharpened focus on the delta's vulnerability to rapid changes in accommodation space (Frihy et al., 2010; Marriner et al., 2012). The subsidence of its coastal area and the sea-level rise scenarios projected by the Intergovernmental Panel on Climate Change (IPCC), potentially threatens one of Egypt's most valuable economic resources (63% of national agricultural land; Hereher, 2010) and the livelihood of >50 million people (Becker and Sultan, 2009). The vulnerability of the Nile Delta will be exacerbated by the significant increase of population density predicted in the next 25 years (Hzami et al, 2021). Presently, >50% of the Nile Delta's inhabitants live on the coast within the first three meters above the present mean sea level (MSL), with population density exceeding 1000 persons per km^2 (Warner et al., 2009). Therefore, every future reduction in the delta surface will likely have a very negative impact on Egypt's livelihood and the delta's overall habitability.

Although the sedimentary records of the coastal margin of the Nile are numerous, the lack of high-resolution study of paleo-environmental change, including hydro-climatically related sediment provenance is evident. The older deltaic promontories provide the unique opportunity to analyse the sensitivity of these coastal morphological features to long-term changes affected by the variations of Nile sediment supply (Stanley and Warne, 1993; Flaux, et al., 2017). Furthermore, diagnostic geochemical proxies can help comprehend sediment sources that have shaped the coastal topography under the land-sea interface (Arbouille and Stanley, 1991; Krom et al., 2002).

Therefore, the purpose of the present study is to examine the Holocene environmental evolution of the Burullus lagoon on the northern-central Nile Delta (Figure 1). The goals of the

study are: 1) to establish the Holocene stratigraphic framework of the Burullus lagoon using high-resolution radiocarbon dating; 2) to understand the sedimentary influences of the old Nile branches on Burullus development through time; and 3) to identify sediment provenances in relation to basin-wide hydro-climate changes by means of diagnostic sediment proxies. The result is to fill in our knowledge gap of the study area.

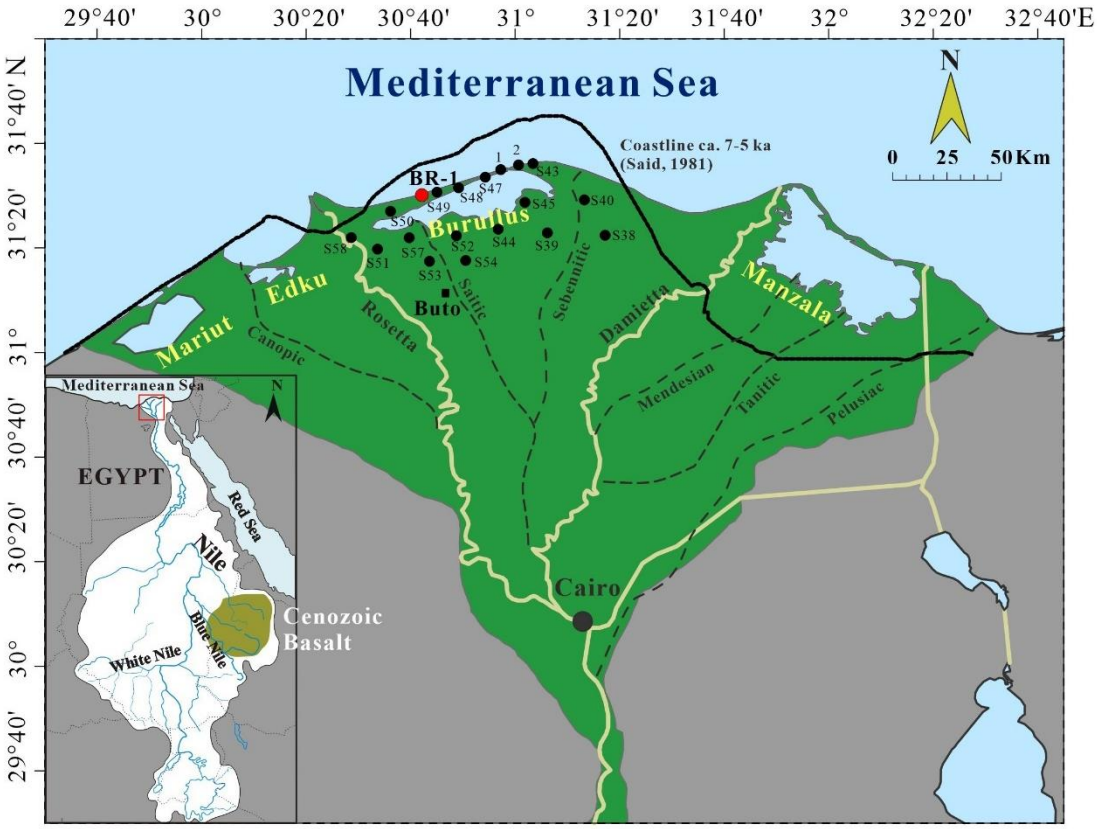

Figure 1: The Nile Delta, showing: 1) Burullus Lagoon and sediment core site BR-1; 2) paleo-coastline of ca. 7-5 ka (after Said, 1981); 3) paleo-Nile branches (Said, 1981), and 4) sediment cores collected from previous studies (Core 1-2 from Sestini, 1989; S-cores from Arbouille and Stanley, 1991). The basaltic distribution of the Blue Nile was after Revel et al. (2010). Square in black shows the archaeological site of Buto (discussed in text).

2. Geomorphological setting

The Nile Delta has experienced a dramatic morphological change during the Holocene. This is reflected by important displacements of the coastline and by the disappearance of several fluvial branches. Between the Roman annexation of Egypt (1st century BC) and the early Arab period (7th century AD), the Nile Delta underwent a major reshaping of its

hydrology. It evolved from seven major branches to two, namely the current Rosetta (on the west) and Damietta (on the east) branches (Butzer, 1976; Said, 1993; Figure 1). These branches remained active mostly during the Early-Middle Holocene, in transporting fluvial sediment out of gorges at Cairo to the delta coast. Their wax and wane often resulted not only in morphological change of the delta plain, but also large-scale shift of the coastline (Buter, 1976). In context of human scale, these changes were a long process. However, on the Holocene scale they happened at a very rapid pace, linking to a period of climate warming, rising sea level, rapid subsidence of the deltaic plain and human interferences (Stanley and Clemente, 2017).

The Burullus lagoon is a shallow (depth <2 m; Mohamed et al., 2016) elongated water body separated from the sea by a sand spit through the remobilisation of sediments transported to the coast by the Rosetta branch and the erosion of the Rosetta promontory. The lagoon is presently connected to the sea by an artificially maintained narrow channel at its eastern margin. This lagoon lost 62.5% of its area between 1801 and 1997 (Shaltout and Khalil, 2005) and ca. 43% of its open water area due to severe anthropogenic activities in recent decades (El-Asmar et al., 2013). The sediment core BR-1 was collected on the northern shore of the Burullus lagoon located in the northern-central Nile Delta (Figure 1). Previous studies have highlighted that the Holocene deltaic sedimentary sequence, which covers the marine transgressive sands of Early-Holocene age, is 10-26 m thick. Deltaic deposits are composed of a succession of lagoonal, marshy and fluvial sediments deposited after 8.0-7.5 ka. In the northern part of the lagoon, these deposits are covered by a <6 m thick sandy unit, corresponding to the presence of the sand spit since ca. 3-4 ka (Arbouille and Stanley, 1991).

3. Material and methods

3.1. Sediment coring, logging and sampling

The sedimentary core BR-1 was drilled using a rotary corer (Figures 1 and 2). Sediment was collected continuously by a 1-m long corer with a diameter of 9 cm. BR-1 (19.2 m long: 31°28'3.025'' N; 30°39'49.662'' E; +2 m MSL) was stratigraphically described in the field. Sediment samples were kept in wooden boxes and transported to the laboratory at Kafrelsheikh University (Egypt). The sediment core was split into two halves, one for sampling and the other for archiving. Core sediment was logged for its colour, stratigraphy, water content, biogenic content (complete shells and shell debris) and mineral distribution. In total,

65 samples were taken at ca. 30 cm sampling interval. Each sample was divided in two parts, for bio-sedimentology and geochemistry. Analyses were performed in the Geography and Archaeology laboratories at Durham University (UK). Samples were freeze-dried and grounded for magnetic susceptibility, X-ray fluorescence (XRF) and carbon measurements. We have further compared our analytical results with other data from the Burullus region to understand the paleo-geographical changes of the lagoon (Wunderlich, 1988; Arbouille and Stanley, 1991).

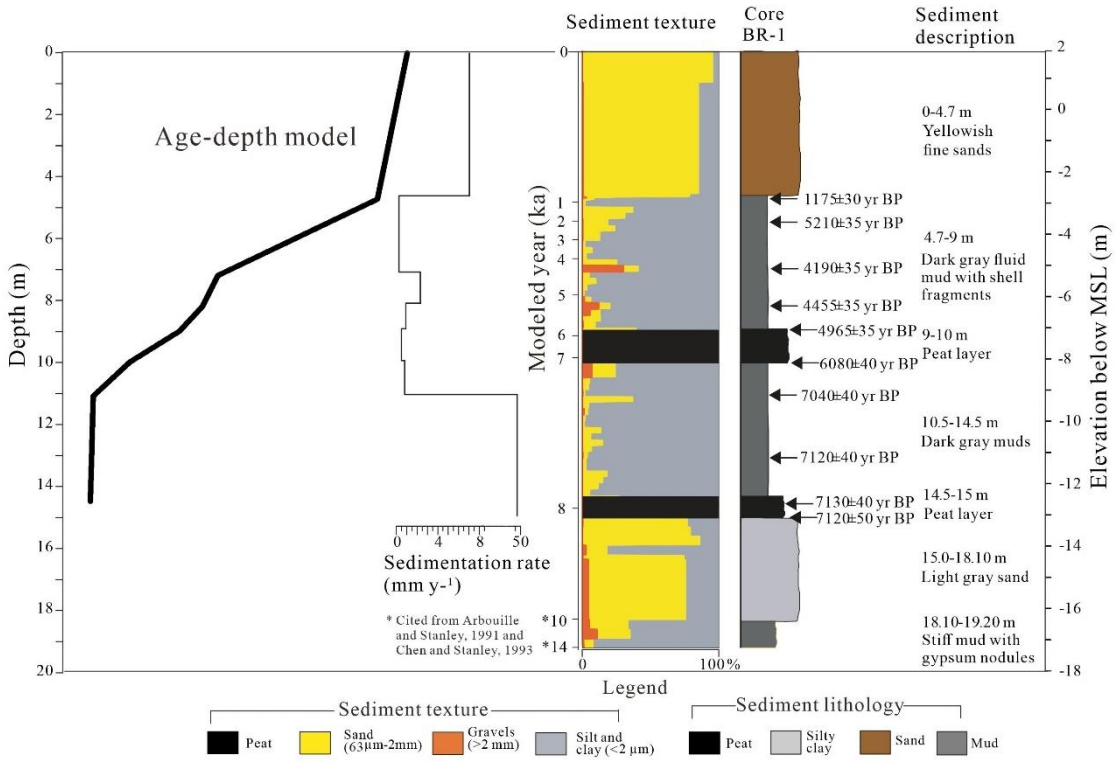

Figure 2: AMS-^{14}C-dated Holocene sediment sequences of BR-1. The age-depth model was reconstructed using the dedicated R-code Clam (Blaauw, 2010) and sedimentation rates were calculated.

3.2. Radiocarbon-dating

Ten (10) AMS-radiocarbon measurements were performed at the Poznan Radiocarbon Laboratory (Poland) on plant remains, seed, charcoal remains, bulk sediment or articulated mollusc shell (Table 1). The age obtained from articulated mollusc shell (*Cerastoderma glaucum*), was corrected using a marine reservoir age of 400 years. Using seven ^{14}C dates (Table 1; Figure 2), we constructed an age-depth model for BR-1 using the dedicated R-code Clam (Blaauw, 2010). We did not use three available datings. One was age-inversion at 5.4-5.5

m depth for which the age is older than the dating at 7.1-7.2 m depth (Figure 2). Between 12.9-14.9 m depth came with three similar ages from different samples measured. We rejected two of them; one at 14.9 m depth (7120 ± 50 BP) because the dated sample (seed) had lower carbon content (0.3 mgC) and another at 13 m depth (7120 ± 40 BP) because of bulk sediment used.

All conventional dates were calibrated using the Calib Rev 8.20 program with the IntCal20 calibration curve (Stuiver and Reimer, 1993; Reimer et al., 2020). Dates were given at confidence intervals of 95.4% (2σ) in years before present (cal. yr BP), simply used as ka in present study.

Table 1. Details of AMS-^{14}C-dating materials of BR-1. ^{14}C dates were expressed in calibrated years BP at the 95% confidence level (2σ). Accepted ^{14}C dates were used for Age-depth model

Sample No.	Lab. No.	Materials	Sampling depth (m)	Age ^{14}C (yr BP)	Calibrated age (cal. yr BP, 2σ)	Remarks
BR-1 470-473	Poz-107202	Marine shell (*Cerastoderma glaucum*)	4.70-4.73	1175±30	700±30	Accepted
BR-1 540-550	Poz-107382	Organic material	5.40-5.50	5210±35	5670±222	Rejected (reworked material)
BR-1 710-720	Poz-107238	Plant remains	7.10-7.20	4190±35	4710±130	Accepted
BR-1 810-820	Poz-107239	Charcoal	8.10-8.20	4455±35	5130±155	Accepted
BR-1 890-900	Poz-107384	Peat	8.90-9.00	4965±35	5725±125	Accepted
BR-1 980-1000	Poz-107385	Peat	9.80-10.00	6080±40	6925±225	Accepted
BR-1 1090-1110	Poz-107240	Plant remains	10.90-11.10	7040±40	7612±195	Accepted
BR-1 1290-1300	Poz-107456	Organic sediment	12.90-13.00	7120±40	7688±204	Rejected (bulk sample)
BR-1 1440-1450	Poz-107241	Plant remains	14.40-14.50	7130±40	7945±80	Accepted
BR-1 1480-1490	Poz-107386	Seed	14.80-14.90	7120±50	7690±210	Rejected (0.3 mgC)

3.3. Dated peat and lagoon muds for Holocene sea-level reconstructions

Two-^{14}C dates of peat layers and three ^{14}C dates of lagoon muds were used to reconstruct the Holocene sea level (Figure 3). Elevation calibration to MSL was performed, i.e. 2.0 m subtracted from the core depth of peat layer, accounting for the surface elevation at the core site above MSL; 1.5 m (average water depth of lagoon of the Nile Delta) added to the sampling depth in case of lagoon sample. In addition, 13 ^{14}C dates of peat layers of the study area were selected from the study by Arbouille and Stanley (1991) for the sea level simulation (Figure 3). The same elevation calibration was also applied to these radiocarbon dates. The sea-level curve was calculated using the best-fit approach.

3.4. *Bio-sedimentology*

The general texture of the sediment, including the gravel (>2 mm), sand (63 µm–2 mm) and silty-clay (<63 µm) fractions, was determined by wet sieving ~50 grams of oven-dried sediments. Ostracods were picked from the >125 µm fraction. Mollusc shells were identified in the gravel fraction according to D'Angelo and Garguillo (1978).

3.5. *Magnetic parameters*

Magnetic susceptibility (MS) measurements were undertaken using a Bartington MS2B magnetic susceptibility meter using a dual frequency sensor. Milled freeze-dried sediments were placed in 10 ml pre-weighted cylindrical plastic containers. MS was measured three times for each sample, both at low (0.465kHz ± 1%) and high frequencies (4.65kHz ± 1%). Mean MS values were corrected to consider mass differences between measured samples and samples used for calibration. Measurements are reported as mass-specific magnetic susceptibility in SI units ($\times 10^{-8} m^3.kg^{-1}$).

3.6. *Geochemical element analyses*

Geochemical elements (Al, Fe, Ti, Cr, Zr, Hf, both major and trace) were measured on ball-milled samples. The homogenised bulk sediment sample 0.6 g was mixed with 6 g of flux (66.67 % Lithium Tetraborate, 32.83 % Lithium Metaborate and 0.50 % Lithium Iodide) and fused to a glass disc using a Claisse LeNeo fusion instrument. Major and trace elements were then determined using a Panalytical Zetium X-Ray Fluorescence Analyser (XRF). We checked the accuracy by international standard reference material and replicates of analyses of

selected samples. Fe, Ti and Cr (mafic proxy) were selected considering the nature of basaltic exposures in the Blue Nile watershed (Krom, et al., 2002; Marshall et al., 2011; Chen et al., 2020), and Zr and Hf (felsic proxy) as a tracer of the Precambrian crystalline base of the While Nile (Revel et al., 2010; Gu et al., 2014; Chen 2020). These elements were normalized to Al in order to minimize grain-size effects (Chen et al., 2010). The total bulk sediment elemental composition is presented in the Supplementary data (seeing Supplementary Material). XRF was not measured on peat samples to avoid the possible impact of organic matter on the geochemical composition of the sediments.

3.7. Carbon content

Total inorganic carbon (TIC) has been measured using an Analytik Jena Multi EA (Elemental Analyser) 4000. Milled freeze-dried sediments were weighed in ceramic cups and introduced in turn into the instrument via an autosampler. For TC analysis, samples are combusted at 1000 - 1500°C in the presence of oxygen without the use of a catalyst. Samples for TIC analysis were first treated with 40 % Orthophosphoric acid to remove the organic carbon component before being combusted. In both cases the gas generated from the burning of the sample is detected by a NDIR (Non-Dispersive Infrared) detector. TOC is then determined by the instrument from the difference between TC and TIC values.

4. Results

4.1. Chronology, sedimentation rate and Holocene sea level curve

The 7 AMS-datings of BR-1 provide a chronological framework from ca. 8.0 to ca. 0.7 ka BP (Table 1, Figure 2). In addition, considering absence of ^{14}C dating at the basal section of the core, we inferred an age of ca. 10 ka for the Holocene bottom sediment section, and ca. 14 ka for the Late Pleistocene stiff muds (Figure 2,4,5), according to the substantial chronostratigraphic data produced by previous studies (Arbouille and Stanley, 1991; Chen et al., 1992; Chen and Stanley 1993). ^{14}C datings were used to calculate the sedimentation rate of BR-1, showing an extraordinarily high rate (50 mm/yr) between the core depth 14.5-11 m, and the lower rate (0.6-2.3 mm/yr) between 11-4.7 m, and higher rate (7.2 mm/yr) between 4.7-0 m (Figure 2). The reconstructed Holocene sea-level curve of the study area indicates that the sea level was 14 m below MSL at 8 ka, and then quickly rose to 4 m below MSL at 6 ka, before approaching the present MSL (Figure 3).

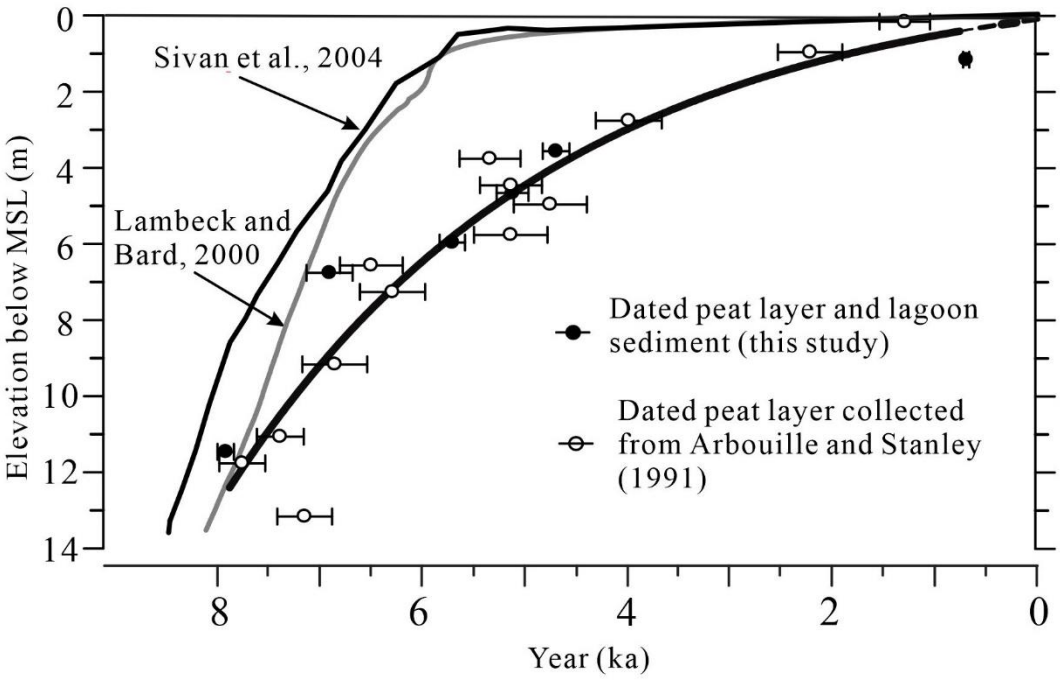

Figure 3. Reconstructed relative sea level of Burrulus coast, using both dated peat layers and lagoon muds from this study and dated peat layers from Arbouille and Stanley (1991).

4.2. Bio-sedimentology of core BR-1

The sedimentary sequence of core BR-1 constitutes a classic transgressive-retrogressive sequence (Reineck and Singh, 1975; Figure 2). The sequence broadly displays three main sedimentary textures; silty-clay between 19.2-18.8 m, between 14.5-10 m and then between 8.8-4.7 m; from fine-to-medium sands between 18.8-15 m and then between 4.7-0 m. Two organic-rich peat layers are intercalated in the sequence (between 15.0-14.3 m and between 10.0-8.8 m).

Most of the sediment samples are devoid of fauna. Only valves of the ostracod *Cyprideis torosa* were found in variable quantity in the upper section of the core (7-4.6 m; Figure 4). Molluscs were also found in nine samples of the upper core sediment (Figure 4), represented by lagoonal *Cerastoderma glaucum* shells (n=8). The upper part of the core also shows the presence of shells living in infralittoral environments such as *Bittium reticulatum* (n=1), *Jujubinus* sp. (n=1) and *Rissoa* sp. (n=1).

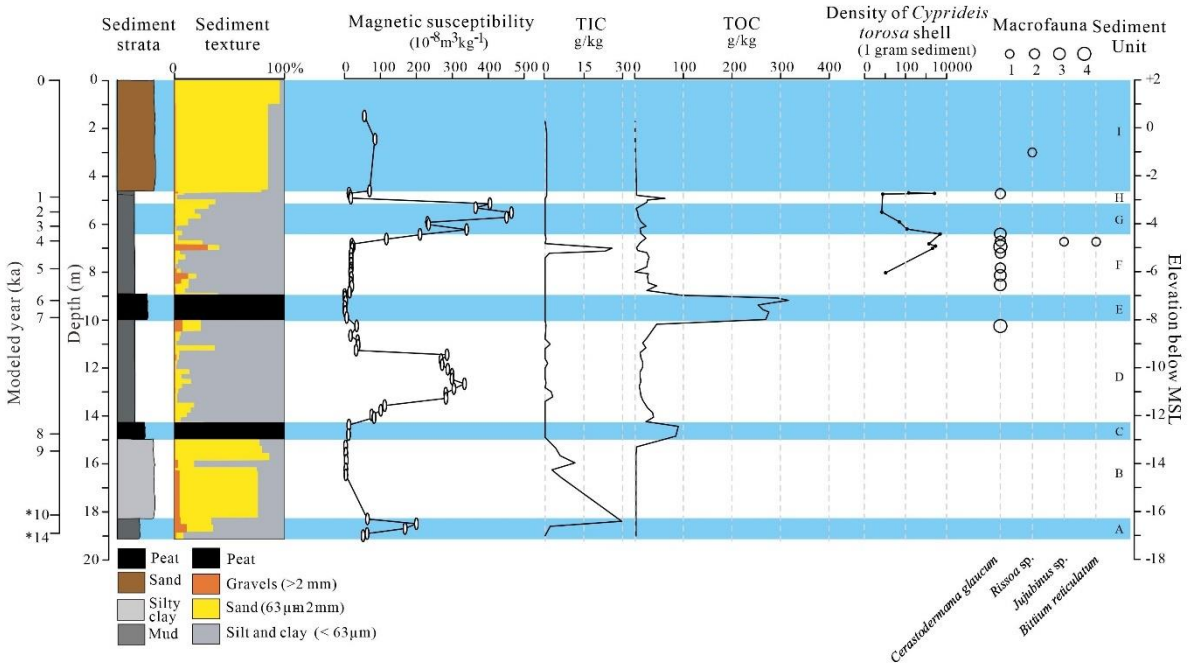

Figure 4: Distribution of sediment magnetic susceptibility (MS), TIC, TOC, macro-fauna and ostracod of core BR-1. Our data were used to define nine sedimentary units (A-I). * - age cited from Arbouille and Stanley (1991) and Chen and Stanley (1993)

4.3. Magnetic susceptibility

Magnetic susceptibility (MS) values are non-uniform along the sedimentary profile and vary from $1.10^{-8}m^3/kg^{-1}$ to $468.10^{-8}m^3/kg^{-1}$. Two MS peaks ($14.10^{-8}m^3/kg^{-1}$ to $468.10^{-8}m^3/kg^{-1}$ at 11.4-13.3 m and $233\text{-}468.10^{-8}m^3/kg^{-1}$ at 6.3-5.2 m) occurred in the Holocene muddy sediment section (Figure 4), separated by the markedly low MS throughout. MS variations can often be subject to sediment provenances from the mother rocks of river basin, nevertheless post-sedimentary diagenesis is also possible.

4.4. Carbon content

Both total inorganic carbon (TIC) and organic carbon (TOC) values are not consistent along the core profile (Figure 4). TIC values are typically <3 g/kg with some exceptions in the basal core sediment and around 7 m depth (Figure 4). TOC values are also markedly low (10-15 g/kg) in BR-1 sediments, except the peat layers (60-300 g/kg).

4.5. Geochemical element distribution

The results of the XRF analysis of diagnostic geochemical elements (Al, Fe, Ti, Cr, Zr, Hf) used in the study were shown in Figure 4 (seeing raw data in Supplementary Material). Almost all elements had kept their distribution pattern with Al (Figure 5), apparently due to grain-size effect (Chen et al., 2020). Fe, Ti, Cr and Hf showed decreasing values from 14- 8 ka, while Zr shows a minor increase (Figure 5). After this, all elemental values rose until ca. 2 ka, in addition to Hf, which had kept its fluctuations in the same time. Interestingly, after normalization to Al (Figure 5), Fe/Al and Ti/Al show similar trends throughout the Holocene, while Cr/Al is also lightly correlated with the pattern. In general, Fe/Al, Ti/Al and Cr/Al show higher values after 8 ka with two co-highs to MS during ca. 7.8-7.3 ka and 3.5-2.0 ka (Figure 5). In comparison, Zr/Al and Hf/Al were markedly high before 8 ka, before being superseded by Fe/Al and Ti/Al from 8.0-2.0 ka (Figure 5). Since then, Zr/Al and Hf/Al were lower. Geochemical results of the sandy section of the core top (<2.0 ka) are not discussed here.

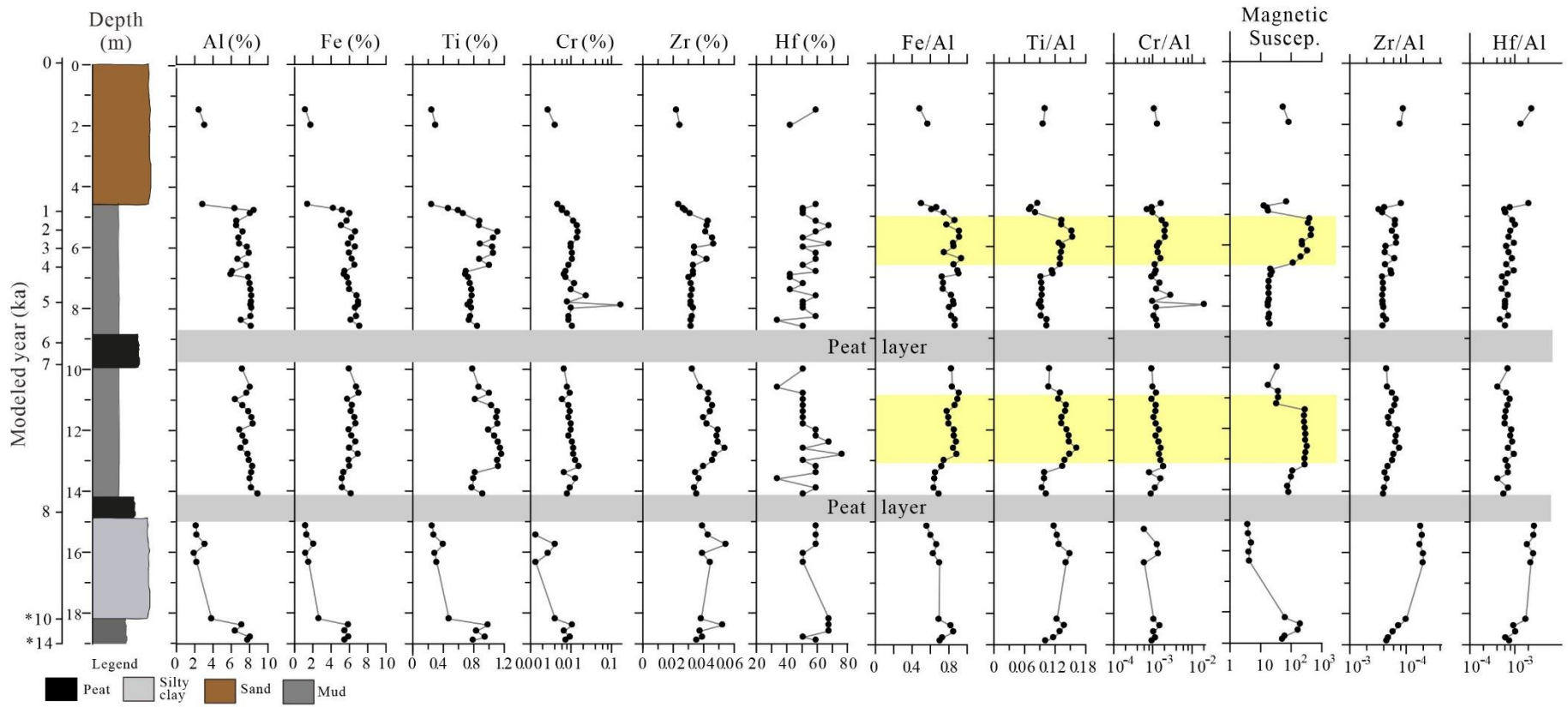

Figure 5: Diagnostic geochemical elements (Al, Fe, Ti, Cr, Zr, Hf) and their normalized values (to Al) of core BR-1 (data from the peat layers are not included). Magnetic susceptibility (MS) is listed for comparison. * - age cited from Arbouille and Stanley (1991) and Chen and Stanley (1993)

5. Discussion

Using multiple proxies from sediment cores to reconstruct the paleo-environmental change can serve as a robust approach to enhance understanding of the Holocene evolution of deltas (Coleman et al., 1998; Reitz et al., 2015). Our well-dated BR-1 sediment data attests to this.

5.1. Coastal paleo-environmental changes: transgressive and retrogressive sequences

The nine paleo-environmental units of BR-1 (A to I) can be identified (Figure 2,4), namely units A-D the transgressive sequence, and units E-I the retrogressive sequence. These units, from core-bottom to top, highlight the morphodynamic evolution of Burullus lagoon during the Holocene.

5.1.1. Unit A – over bank deposits: 19.2-18.2 m (14-12 ka)

This unit is composed of brownish stiff muds of Late Pleistocene age (Figure 4; Chen and Stanley, 1993). MS values vary from 53 SI to 202 SI (Figure 4). Calcareous nodules and higher TIC (30 g/kg) are observed, both reflecting the evaporation setting of the Late Pleistocene in the NE Africa (Chen and Stanley, 1993). Previous works (Elliott, 1974; Arbouille and Stanley, 1991; Chen and Stanley, 1993) have associated similar deposits formed by the Nile channel overbank processes in the area, dating to ca. 14-10 ka (Stanley and Warne, 1993), when the sea level was much lower than today.

5.1.2. Unit B - marine/estuarine transgression: 18.2-15 m (before 8.0 ka)

A 3.2 m thick sandy unit overlies the overbank deposits. This unit is homogeneous, mainly composed of greyish fine sand (80-86%). The gravel fraction (<4 %) consists of small calcareous nodules and marine shell fragments. MS values are lower in this unit (4-5 SI) (Figure 4). Two ^{14}C dates obtained from the peat sediment on the top demonstrate that the sandy section developed before ca. 8 ka (Figure 2). This section was the reworked product of the earlier marine and shallow-marine shelf sediments, which were mostly deposited between 12.0-7.5 ka in the Burullus area (Arbouille and Stanley; 1991). Flaux et al. (2017) interpreted a similar deposit in the nearby Abukir Bay (west of the Rosetta promontory) and found this environment consistent with a euryhaline estuarine/coastal setting before ca. 7.0 ka. Unit B

usually represents the maximum marine transgression of the Early Holocene in the study area, and the coastline was further south of the coring site (Arbouille and Stanley, 1991).

5.1.3. Unit C - salt-marshland: 15-14.3 m (ca. 8 ka)

Unit C is composed of peat sediment rich in organic matter and with lower MS values (11-12 SI) (Figure 2, 4). The unit is dated to ca. 8 ka (age-depth model; Figure 2), corresponding to the development of a costal marshland when sea-level rise began to stabilize. It developed at an elevation of 13 m below MSL (Figure 2). Coastal marshland was widely developed on the back of central-west of Burullus lagoon, which enables to be used for the Holocene sea-level reconstruction (Figure 3; discussed below) (Arbouille and Stanley, 1991).

5.1.4. Unit D - open bay with higher fluvial inputs: 14.3-10.0 m (ca. 8.0-7.0 ka)

Unit D comprises brownish grey muds (63-99%) and is devoid of fauna. Higher MS values (271-336 SI) were recorded in the middle of this unit (Figure 4). Flaux et al. (2017) have described high MS for the nearby Edku lagoon, and associated them with high fluvial inputs referring to the similar range of MS values measured in the Late-Holocene floodplain muds of the Nile (100-470 SI) (Ghilardi and Boraik, 2011). In addition, higher mica content seen under binocular microscope is in accordance with the composition of modern fluvial samples (Stanley and Chen, 1991). Unit D can be interpreted as an open bay before sea level reached its maximum level. The markedly high sedimentation rate (50 mm/yr, Figure 2) of the unit translates an episode of high deposition, most likely affected by the paleo-branches of the Nile that prevailed on the Burullus coast in the Early-Middle Holocene (Buzter, 1976).

5.1.5. Unit E - salt-marshland: ca. 10.0-8.9 m (ca. 7.0-5.7 ka)

Like unit C, unit E consists of peat sediments rich in organic matter, indicating a deceleration of sea-level rise during the Early-Middle Holocene (Figures 2, 4). The formation of this peat layer translates the seaward position of the coastline at ca. 7-5.7 ka (Figure 2). Wunderlich (1988) has described a marshy area, dated from 6 to 4.5 ka, which extended further inland around the archaeological site of Buto, ca. 30 km south of the coring site. The development of a marshy environment in this area can be linked to a decrease in sediment inputs from the river or a channel avulsion. Revel et al. (2015) show that the decrease in Nile terrigenous inputs to the western pro-delta occurred during the first half of the 7th millennium

BP. The base of this peat layer dated to ca. 7 ka at 8 m below MSL was used to reconstruct the sea-level rise history of the study area (Figure 3; discussed below).

5.1.6. Unit F - lagoon environment: 8.90-6.30 m (ca. 5.7-3.2 ka)

Unit F is dated to ca. 5.7-3.2 ka (Figure 2). This unit is characterized by lower and homogenous MS values (15-24 SI). In the unit, a high abundance of *Cyprideis torosa* (up to 2680 individual/1-g sediments) is observed. They are associated with lagoonal molluscs (*Cerastoderma glaucum*) and some marine species (*Jujubinus* sp. and *Bittium reticulatum*). This demonstrates that the former transgressive and open marine setting (unit D) was transformed to an open lagoon environment after ca. 5.7 ka, as part of retrogressive process. Previous work has shown the same succession, with a lagoonal environment covering a salt-marshy layer in the Burullus and Edku coast (Wunderlich, 1988; Arbouille and Stanley, 1991; Chen et al. 1992; Flaux et al., 2017). The lower sedimentation rate of this unit indicates less fluvial input to the lagoon during this time period (Figure 2).

5.1.7. Unit G - fluvially-affected lagoon: 6.3- 5.15 m (ca. 3.2-1.5 ka)

Unit G is the same sediment texture as unit F. It is dated to 3.2- 1.5 ka (Figure 2). However, this unit presents higher MS values (234-410 SI) consistent with the presence of mica in the sand fraction. Lagoonal fauna disappear, along with a decrease in the density of the ostracod *Cyprideis torosa*. Nevertheless, the persistence of the ostracod demonstrates that the lagoon was still partially connected to the sea. In this unit, we observed an inverted date at core depth 5.4 m (Table 1), which may be consistent with the deposition of reworked older organic matter via river transport. Probably, a negative sedimentary budget leading to a marine intrusion into the Canopic promontory was identified between 3.5-2.0 ka (Flaux et al., 2017). While a lowering of Nile flow during this period was widely documented (Marriner et al., 2012), the negative sedimentary budget identified in the area of the Canopic branch may result in from the partial the shift of the river branch towards the east of the Burullus area.

5.1.8. Unit H - closing lagoon: 5.15-4.70 m (ca. 1.5-0.7 ka)

Unit H highlights the brief development of a lagoon, but much more isolated from the sea because of the growing sand spit (Figure 2). Increasing ostracod (*Cyprideis torosa*) density

(132-2300 individual/1-g sediment) is observed (Figure 2, 4), perhaps due to more saline water under reduced Nile flow during the post-AHP climate aridification (Zhao et al., 2020).

5.1.9. Unit I - sand spit: 4.70 – 0 m (0.7 – 0 ka)

Unit I consists of thicker sand section on the top of BR-1 (Figure 2), with small calcareous gravels in the lower part of this unit. This unit corresponds to the development of the sand spit along Burullus coast as of ca. 3-4 ka (Arbouille and Stanley, 1991). The sand spit formed because of reworking of sediments via coastal currents, as the water and sediment supply from the upper basin dramatically decreased under the drying climate in the Late Holocene (Marriner et al., 2013; Zhao et al., 2020).

5.2. Palaeoenvironmental evolution of Burullus lagoon: multi-proxy implications

The multiple sediment proxies of BR-1 used in this study can help comprehend the Holocene environmental change of the Nile Delta, including hydroclimate-related sediment provenances, sea-level rise and coastal morphodynamical processes.

5.2.1. Sediment provenances and sedimentation rate: hydroclimate implications

Diagnostic geochemical elements of BR-1 selected in this study are meaningful in reflecting sediment provenances of mother rocks of the Nile River basin (Figure 5). Ti and Cr (mafic origin) can be used to trace sediment provenance from the Blue Nile where basaltic exposures are dominant (Krom et al., 2002; Revel et al., 2010; Gu et al., 2014). High Fe content was also linked to the Blue Nile source (Krom et al., 2002). Zr and Hf can commonly refer to the felsic nature of a sediment source (Gu et al., 2014; Chen et al., 2020), and thus can be linked to the White Nile, where Precambrian crystalline bedrock prevails (Revel et al., 2010). Of note, this source-sink inter-correlation using same diagnostic geochemical elements as this study has been established in the Changjiang River catchment and on the southeast China coast, recently (Gu et al., 2014; Chen et al., 2020).

As mentioned before, the elemental values of bulk samples are inevitably affected by the proportion of fine grain size (Figure 5). However, after normalization to Al (grain-size proxy), our results show the coherent interlinkage of source-sink (Figure 5).

The synchronous increase in Fe/Al, Ti/Al, Zr/Al, Hf/Al in the sediment profile of BR-1 before ca. 8 ka (Figure 5) indicates sediment provenance both derived from the White Nile

and the Blue Nile during the main AHP. Since then, Fe/Al and Ti/Al (Cr/Al is also lightly correlated), had kept their ascending values up the core with two increases. This was asynchronous to non-fluctuated Zr/Al and Hf/Al in BR-1 (Figure 5). The higher Fe/Al, Ti/Al and Cr/Al can be attributed to the increasing sediment source from Blue Nile, since a less vegetated basaltic surface suffered from intensive erosion due to the southerly shifting ITCZ (Krom and Stanley, 2002; Revel et al., 2010). Our Fe/Al and Ti/Al vs. reduced $^{87}Sr/^{86}Sr$ value measured in sediment core S21 of the Nile Delta reflects the long-term climate aridification and the concomitant increase in sediment flux from the Blue Nile since 6 ka (Figure 6) (Krom et al., 2002). Also, the lowering level of lake Tana in the Blue Nile basin (Ethiopia Plateau) has been evidenced since 8 ka through analysis of δD_{wax} (lake level proxy), confirming the post AHP drying climate, with the similar context of Fe/Al and Ti/Al (Figure 6) (Marshall et al., 2011).

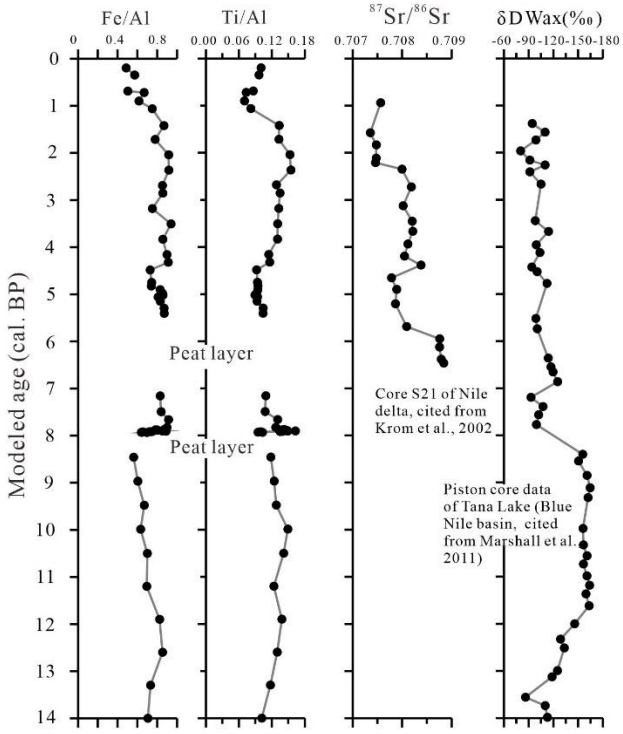

Figure 6: Comparison of Fe/Al and Ti/Al of this study to $^{87}Sr/^{86}Sr$ of core S21 (Nile Delta) and water level proxy (δDWax ‰) of the Blue Nile basin

The two pulses of higher Fe/Al and Ti/Al that were also coeval in distribution to the higher MS recorded in BR-1 profile during ca. 7.8-7.3 ka and 3.5-2.0 ka (Figures 4, 5), suggesting more mafic sediment fluxes to be flooded from the Blue Nile to lagoon coast via paleo-Nile branches prevailed at those times. Ti content is a good indicator for Blue Nile inputs,

since its catchment is characterised by a volcanic (basaltic) nature, especially when it varies synchronously with changes in the magnetic mineralogy (volcanic rocks being enriched in Ti-magnetite) (Marshall et al., 2011).

The lowering sedimentation rate from the previous 50 mm/yr before 8 ka to ca. 1-2 mm/yr between 8-1 ka (Figure 2) was associated to the drying climate setting after the main AHP (Shanahan et al., 2015; Tierney et al., 2017). Virtually, the high sedimentation rate (ca. 7.0 mm/yr) of thicker sand layer on the top BR-1 manifested the intensifying aeolian processes coupled with weakening fluvial sedimentation during the Late-Holocene drying climate condition (Figure 2).

5.2.2. Reconstructed relative sea-level: insights from dated peat layers and lagoon muds

Saltmarshes (peat layer) are often used for reconstructing the Holocene sea level because they form at an elevation corresponding to the contemporary position of mean sea level (Chen and Stanley, 1998; González and Törnqvist, 2009; Wilson, et al., 2020). Our dated peat layers, together with dated lagoon muds can highlight more precisely the sea-level positions of the central Nile coast during the Holocene (Figure 3).

We noted that all reconstructed Holocene sea levels of delta coast are relative ones due to eustatic and isostatic movements. Through comparison, it is demonstrated that our reconstructed sea level that lies -14 m below MSL at 8 ka, and -4 m below MSL at 6.0 ka before gradually approaching the present MSL is similar to that of the Mississippi delta, where higher tectonic subsidence predominates (Tornqvist et al., 2004). Also, our reconstructed sea level curve lies ca. 4-1 m below the relative sea-level curve established for the Mediterranean coast of France and Israel (Figure 3), where tectonic subsidence is thought to be minor (Lambeck and Bard, 2000; Morhange at al., 2001; Sivan et al., 2004, Vacchi et al., 2018). This comparison highlights the considerable land surface lowering that occurred in the central Nile Delta during the Holocene. The compaction rate measured in different part of the Nile Delta are clearly related to the thickness of the Holocene sedimentary sequence mainly formed by fine lagoonal and marsh deposits. Stanley and Clemente (2017) reported subsidence rate of ca. 7.7 mm/yr in the central Nile Delta during the Holocene that can be explained by the thicker lagoonal deposits (>15 m). Higher subsidence rates have been measured in the NE Nile delta where the Holocene sedimentary sequence is 20-40 m think (Stanley and Clemente, 2017).

5.2.3. Morphodynamic impact of the former Nile branches on Burullus lagoon

In the Holocene, there were many paleo-Nile branches flowing through the Nile Delta into the Mediterranean Sea (Figure 1) (Butzer, 1976). The Sebennytic and Saitic branches were the two major branches developed on the eastern and western sides of Burullus lagoon in the Early Holocene (Tousson, 1922; Arbouille and Stanley, 1991). Rapid fluvial sedimentation made the central Nile coast a large-scale promontory-like topography (Figure 1). The coast subsequently suffered from intensive erosion as the branches shifted and diminished during Late Holocene (UNDP/UNESCO, 1978).

BR-1 highlights two major periods with higher fluvial inputs to the Burullus lagoon-coast around 8-7 ka and 3.5-1.5 ka (Units D and G; Figure 4), characterized by the markedly high MS recorded in BR-1 sediment. It is widely acknowledged that fluvial sediment usually contains higher MS derived from soil erosion from river basins (Thompson and Oldfield, 1986), although post-sedimentary diagenesis could be attributable. Here, we would interpret the high MS values of BR-1 as being linked to the stronger fluvial processes of old Nile branches present in the region, in particular, the unit D showing a high sedimentation rate of 50 mm/yr at 8-7 ka (Figure 2, 4). Also, Bernhardt et al. (2012) using terrestrial vegetation identified that high Nile flow occurred before ca. 6.5 ka, as indicated by an increase in Cyperaceae (with *Cladium*) pollen in a core drilled on the southern margin of the Burullus. On the contrary, a reduction in Nile flow and regional precipitation is attested by the decrease in Cyperaceae pollen between ca. 5.2 and 3.5 ka. This period corresponds to an open-lagoonal environment according to the results of the bio-sedimentological study of BR-1.

Marshland was well developed on the central-west Burullus coast (including BR-1 core site) between ca. 8- 4 ka, indicating lower fluvial inputs in the region as identified at both W-E and S-N Holocene sediment transects (Figure 7A,B). During that period, the eastern lagoon coast was deeply incised with fluvial sediment facies via paleo Sebennitic branch sedimentation (Figure 1), as recorded in many sediment cores (Figure 7A) (Sestini, 1989; Arbouille and Stanley; 1991). Subsequently, the established marshland and lagoonal environments were subjected to progressive infilling and reduction in their surface areas (Figure 7A,B; Figure 8a), due to the deposition of fluvial and marine sediments and by the southward displacement of the sand spit. This perhaps was prone to the early human occupation at site of Buto (Tell el-Fara'in), an early cultural center (6 ka, Pre-Dynastic) of Egypt (Ginau et al., 2020), ca. 30 km south to the lagoon coast (Figure 1, 8). The infilling seems to

have been particularly important ca. 3.5-1.5 ka in relation to the presence of several Nile branches flowing into the western area of the lagoon (Figure 8b, c) (Wunderlich, 1988; Wilson, 2012, 2018). In recent time, human activities have made the lagoonal largely shrunk (Figure 8a).

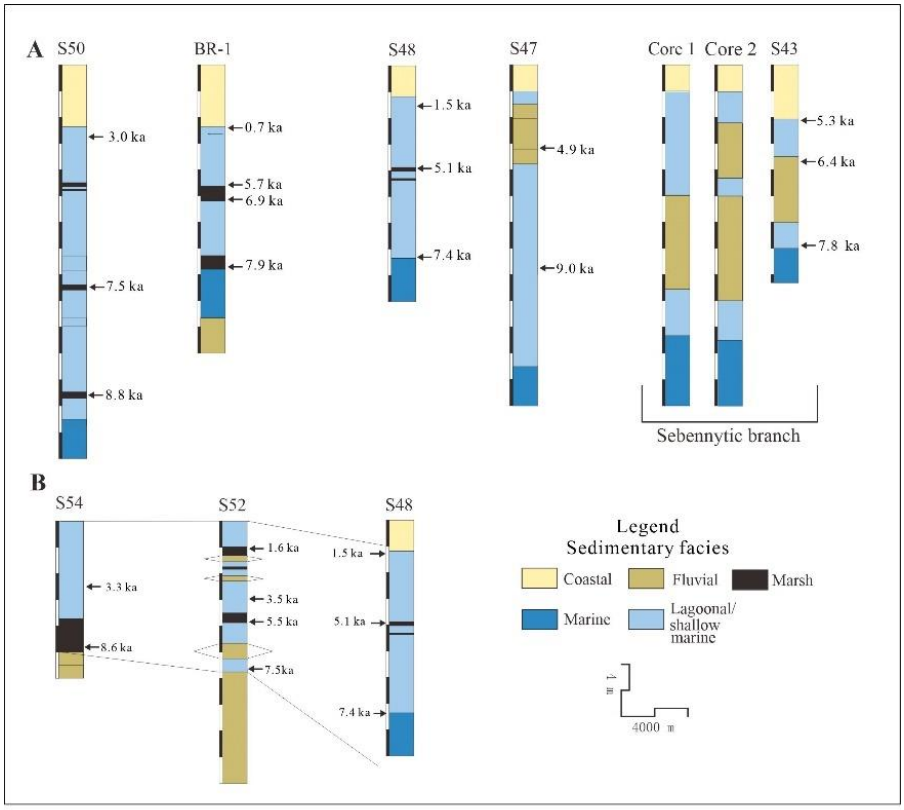

Figure 7: Holocene sediment core transect of Burullus lagoon-coast: A) along-coast; B) perpendicular to coast. Fluvial sediment facies prevail on the eastern lagoon coast, and marshland on the central-west lagoon coast. Holocene sediment core (1-2) and S-cores were collected from Sestini (1989); and Arbouille and Stanley (1991).

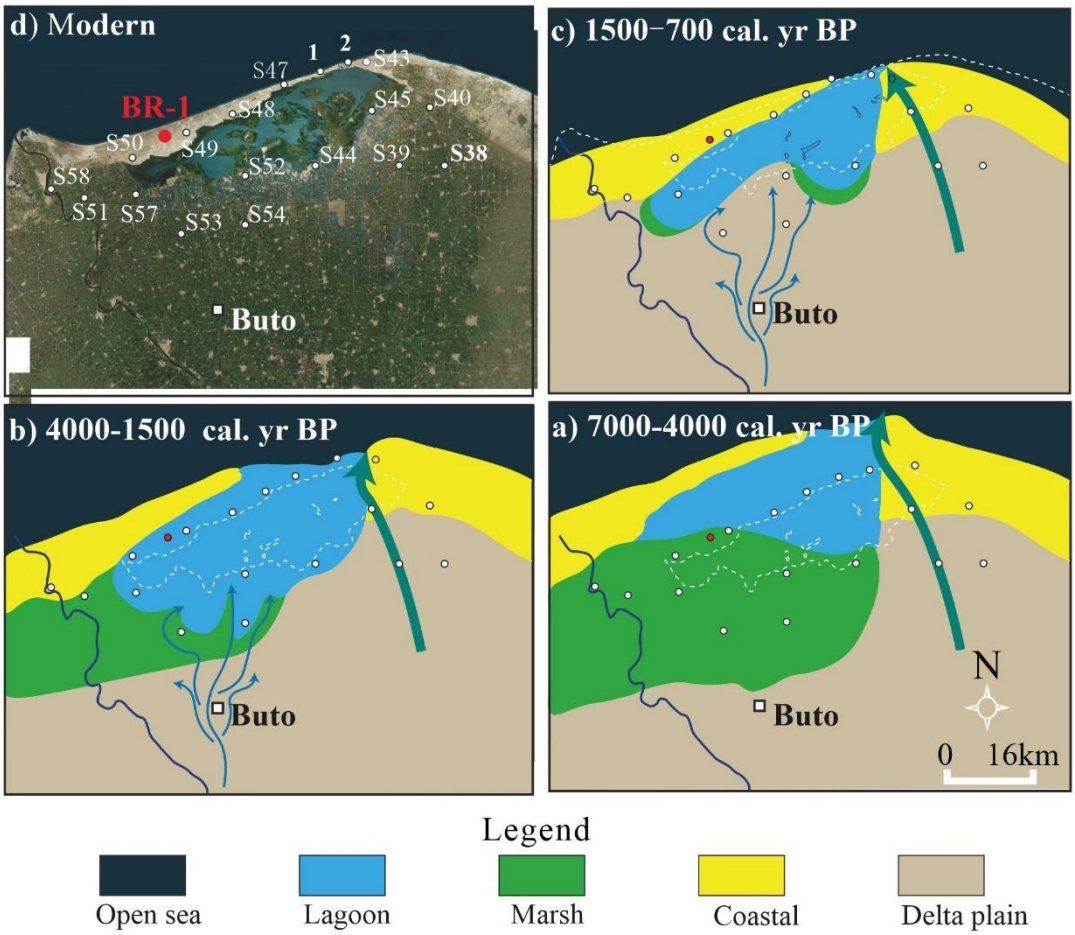

Figure 8 sketch map, showing the Holocene evolution of Burullus lagoon

6. Conclusions

The coastal lagoon of the Nile Delta is an excellent sediment recorder to explore basin-wide hydroclimate change, sea-level rise, source-to-sink sediment transfers, and the history of early cultural development. Our high-resolution study of core BR-1 allows us to make the following conclusions:

1) The Holocene strata of the Burullus lagoon consists of a typical transgressive-retrogressive deltaic sequence, characterized by a marine-estuarine facies (ca. 10-8.0 ka), an open bay facies (ca. 8.0-7.0 ka), a lagoon facies (ca 6.0 ka) and an aeolian facies formed after ca. 1 ka.
2) Two units showing high sediment magnetic susceptibility values are dated to 7.8-7.3 ka and 3.5-2.0 ka in BR-1 show the timing of the main fluvial impact on the lagoon formation.

3) Diagnostic elemental ratios (Fe/Al, Ti/Al, Zr/Al, Hf/Al) showed a synchronous rise before 8.0 ka (the main phase of the AHP), indicating sediment provenances both derived from the White and the Blue Nile watershed. During ca. 8.0-2.0 ka, Fe/Al, Ti/Al, Zr/Al (mafic proxy) maintained an increasing trend with two major fluctuations vs. lightly-fluctuating Zr/Al and Hf/Al (felsic proxy) up the core. This implies more sediment fluxes from the Blue Nile, in relation to the withdrawal of the ITCZ during the post-AHP.

4) Two peat layers (saltwater marsh), dated to ca. 8.0 ka and 7.0-5.7 ka are intercalated with marine-bay and lagoon sediments. Both dated peat and lagoon sediments, along with data collected during previous studies, allowed us to reconstruct the RSL history of the study area. The reconstructed local sea level curve shows that the evaluation of sea level was ca. 4-1 m lower than the reconstructed analogues on tectonically stable coasts during the Holocene, implying an important effect of land surface lowering (most likely sediment compaction) on relative sea level changes.

Acknowledgments

We thank the Departments of Archaeology and Geography at Durham University; in particular Dr. Kamal Badreshany, Martin D. West and Amanda J. Hayton for their help during the analyses.

Funding

M.G was supported by a Durham Junior Research Fellowship co-funded by the European Union under grant agreement number 609412. The project is financially supported by the China National Natural Science Foundation (Grant No. 41620104004). This work received further funding from the CEREGE laboratory (APIC Recherche 2018, CM).

References

Anthony, E. J., Marriner, N., Morhange, C. (2014) Human influence and the changing geomorphology of Mediterranean deltas and coasts over the last 6000 years: From progradation to destruction phase?. *Earth-Science Reviews* 139, 336-361.

555 Arbouille, D., Stanley, D.J. (1991) Late Quaternary evolution of the Burullus lagoon region,
556 north-central Nile Delta, Egypt. *Marine Geology* 99 (1-2), 45-66.
557 Bar-Yosef, O. (2013) Nile Valley-Levant interactions: an eclectic review. In N. Shirai (ed).
558 *Neolithisation of Northeastern Africa. Studies in Early Near Eastern Production,*
559 *Subsistence, and Environment* 16, 237-247.
560 Becker, R.H., Sultan, M. (2009) Land subsidence in the Nile Delta: inferences from radar
561 interferometry. *The Holocene* 19(6), 949-954.
562 Bernhardt, C. E., Horton, B. P., Stanley, J. D. (2012) Nile Delta vegetation response to Holocene
563 climate variability. *Geology* 40(7), 615-618.
564 Besset, M., Anthony, E. J., Bouchette, F. (2019) Multi-decadal variations in delta shorelines
565 and their relationship to river sediment supply: An assessment and review. *Earth-science*
566 *reviews* 193, 199-219.
567 Blaauw, M. (2010) Methods and code for 'classical' age modelling of radiocarbon sequences.
568 *Quaternary Geochronology* 5(5), 512-518.
569 Brown, S., Nicholls, R.J. (2015) Subsidence and human influences in mega deltas: the case of
570 the Ganges–Brahmaputra–Meghna. *Science of the Total Environment* 527, 362-374.
571 Butzer, K.W. (1976) *Early Hydraulic Civilization in Egypt: A Study in Cultural Ecology*. Chicago.
572 Chen, Z., Warne, A.G., Stanley, D.J. (1992) Late Quaternary evolution of the northwestern Nile
573 Delta between the Rosetta promontory and Alexandria, Egypt. *Journal of coastal*
574 *Research* 8(3), 527-561.
575 Chen, Z., Stanley, D.J. (1993) Alluvial stiff muds (Late Pleistocene) underlying the lower Nile
576 Delta plain, Egypt: petrology, stratigraphy and origin. *Journal of Coastal Research* 9(2),
577 539-576.

578 Chen, Z., Zong, Y.Q., Wang, Z.H., Chen, J., Wang, H. (2008) Migration Patterns of Neolithic
579 Settlements on the Abandoned Yellow and Yangtze River Deltas of China. *Quaternary*
580 *Research* 70 (2), 301-314.
581 Chen, Z., Salem, A., Xu, Z., Zhang, W. (2010) Ecological implications of heavy metal
582 concentrations in the sediments of Burullus Lagoon of Nile Delta, Egypt. *Estuarine,*
583 *Coastal and Shelf Science* 86, 491-498.
584 Chen, Z., Stanley, D.J. (1998). Rising sea level on eastern China's Yangtze Delta, *Journal of*
585 *Coastal Research*, 14 (1), 360-366.
586 Chen, J., Liu, P., Sun, D.D., Zhang, D., Miao, B.D., Chen, J., (2020) Riverine Sediment
587 Geochemistry as Provenance Fingerprints along the Eastern Coast of China: Constraint,
588 Approach, and Application. *Minerals* 10, 29.
589 Coleman, J.M., Roberts, H.H., Stone, G.W. (1998). Mississippi River delta: an overview. *Journal*
590 *of Coastal Research* 14(3), 699-716.
591 D'Angelo, G., Garguillo, S. (1978) *Guida alle Conchiglie Mediterranee,conoscerle, cercarle,*
592 *collezionarle*. Milan: Fabri Editori.
593 Day Jr, J.W., Gunn, J.D., Folan, W.J., Yáñez-Arancibia, A., Horton, B.P. (2007) Emergence of
594 complex societies after sea level stabilized. *Eos, Transactions American Geophysical*
595 *Union* 88(15), 169-170.
596 El-Asmar, H.M., Hereher, M.E., El Kafrawy, S.B. (2013) Surface area change detection of the
597 Burullus Lagoon, North of the Nile Delta, Egypt, using water indices: A remote sensing
598 approach. *The Egyptian Journal of Remote Sensing and Space Science* 16(1), 119-123.
599 Elliott, T. (1974) Interdistributary bay sequences and their genesis. *Sedimentology* 21, 611-
600 622.

601 Flaux, C., Marriner, N., El-Assal, M., Kaniewski, D., Morhange, C. (2017) Late Holocene erosion
602 of the Canopic promontory (Nile Delta, Egypt). *Marine Geology* 385, 56-67.
603 Frihy, O.E.S., Deabes, E.A., Shereet, S.M. Abdalla, F.A. (2010) Alexandria-Nile Delta coast,
604 Egypt: update and future projection of relative sea level rise. *Environmental Earth*
605 *Sciences* 61(2), 253-273.
606 Ghilardi, M., Boraik, M. (2011) Reconstructing the Holocene depositional environments in the
607 western part of Ancient Karnak temples complex (Egypt): a geoarchaeological approach.
608 *Journal of Archaeological Science* 38(12), 3204-3216.
609 Ginau, A., Steiniger, D., Hartmann, R., Hartung, U., Schiestl, R., Altmeyer, M., Seeliger, M.,
610 Wunderlich, J. (2020). What settlements leave behind—pXRF compositional data analysis
611 of archaeological layers from Tell el-Fara'in (Buto, Egypt) using machine learning.
612 *Palaeogeography, Palaeoclimatology, Palaeoecology* 546, 109666.
613 González, J.L., Törnqvist, T.E. (2009) A new Late Holocene sea-level record from the Mississippi
614 Delta: evidence for a climate/sea level connection? *Quaternary Science Reviews* 28, 1737-
615 1749
616 Gu, J.W., Chen, J., Wang, Z.H., Wei, Z.X., Chen, Z. (2014) Geochemical composition and
617 provenance study of the Plio-Quaternary sediments in the Yangtze River mouth:
618 implications for river channelization into the sea. *Geomorphology* 227, 166-173.
619 Hereher, M.E. (2010) Vulnerability of the Nile Delta to sea level rise: an assessment using
620 remote sensing. *Geomatics, Natural Hazards and Risk* 1(4), 315-321.
621 Hzami, A., Heggy, E., Amrouni, O., Mahé, G., Maanan, M., Abdeljaouad, S. (2021) Alarming
622 coastal vulnerability of the deltaic and sandy beaches of North Africa. *Scientific reports*
623 11(1).

624 Kennett, D.J., Kennett, J.P. (2006) Early state formation in southern Mesopotamia: Sea levels,
625 shorelines, and climate change. *Journal of Island & Coastal Archaeology* 1(1), 67-99.
626 Krom, M.D., Stanley, J.D., Cliff, R.A., Woodward, J.C. (2002) Nile River sediment fluctuations
627 over the past 7000 yr and their key role in sapropel development. *Geology* 30(1), 71-74.
628 Lambeck, K., Bard, E. (2000) Sea-level change along the French Mediterranean coast for the
629 past 30 000 years. *Earth and Planetary Science Letters* 175, 203-222;
630 Marshall, M, H., Lamb, H. F., Huw, D., Davies, S.J., Bates, R., Bloemendal, Jan., Boyle, J., Leng,
631 M.J., Umer, M., Bryant, C. (2011) Late Pleistocene and Holocene drought events at Lake
632 Tana, the source of the Blue Nile. *Global and Planetary Change* 78, 147-161
633 Marriner, N., Flaux, C., Morhange, C., Kaniewski, D. (2012) Nile Delta's sinking past:
634 Quantifiable links with Holocene compaction and climate-driven changes in sediment
635 supply? *Geology* 40(12), 1083-1086.
636 Marriner, N., Flaux, C., Morhange, C., Stanley, J.D. (2013) Tracking Nile Delta vulnerability to
637 Holocene change. *PLoS One* 8(7), p.e69195.
638 Mohamed, H., Negm, A., Zahran, M., Saavedra, O.C. (2016) Bathymetry determination from
639 high resolution satellite imagery using ensemble learning algorithms in Shallow Lakes:
640 case study El-Burullus Lake. *International Journal of Environmental Science and*
641 *Development* 7(4), 295-301.
642 Morhange, C., Laborel, J., & Hesnard, A. (2001). Changes of relative sea level during the past
643 5000 years in the ancient harbor of Marseilles, Southern France. *Palaeogeography,*
644 *palaeoclimatology, palaeoecology* 166(3-4), 319-329.
645 Perşoiu, A., Lonita, M., Weiss, H. (2019) Atmospheric blocking induced by the strengthened
646 Siberian High led to drying in west Asia during the 4.2 ka BP event – a hypothesis. *Climate*
647 *of the Past* 15, 781-793.

Reineck, H.E., Singh, I.B. (1975) *Depositional Sedimentary Environments*. Springer-V, Berlin.

Reitz, M.D., Pickering, J.L., Goodbred, S.L., Paola, C., Steckler, M.S., Seeber, L., Akhter, S.H. (2015) Effects of tectonic deformation and sea level on river path selection: Theory and application to the Ganges-Brahmaputra-Meghna River Delta. *Journal of Geophysical Research: Earth Surface* 120(4), 671-689.

Reimer, P. J., Austin, W. E. N., Bard, E., Bayliss, A., Blackwell, P. G., Bronk Ramsey, C., Butzin, M., Cheng, H., Edwards, R. L., Friedrich, M., Grootes, P. M., Guilderson, T. P., Hajdas, I., Heaton, T. J., Hogg, A. G., Hughen, K. A., Kromer, B., Manning, S. W., Muscheler, R., Palmer, J. G., Pearson, C., van der Plicht, J., Reimer, R. W., Richards, D. A., Scott, E. M., Southon, J. R., Turney, C. S. M., Wacker, L., Adolphi, F., Büntgen, U., Capano, M., Fahrni, S. M., Fogtmann-Schulz, A., Friedrich, R., Köhler, P., Kudsk, S., Miyake, F., Olsen, J., Reinig, F., Sakamoto, M., Sookdeo, A. Talamo, S. (2020) The IntCal20 Northern Hemisphere radiocarbon age calibration curve (0-55 cal kBP). Radiocarbon 62(4), 725-757.

Renaud, F. G., Syvitski, J. P., Sebesvari, Z., Werners, S. E., Kremer, H., Kuenzer, C., Ramesh, R., Jeuken, A., Friedrich, J. (2013) Tipping from the Holocene to the Anthropocene: How threatened are major world deltas?. *Current Opinion in Environmental Sustainability* 5(6), 644-654.

Revel, M., Ducassou, E. Grousset, F.E., Bernasconi, S.M., Migeon, S., Revillon, S., Mascle, J., Murat, A., Zaragosi, S., Bosch, D. (2010) 100,000 Years of African monsoon variability recorded in sediments of the Nile margin. *Quaternary Science Reviews* 29, 1342-1362.

Revel, M., Ducassou, E., Skonieczny, C., Colin, C., Bastian, L., Bosch, D., Migeon, S. Mascle, J. (2015) 20,000 years of Nile River dynamics and environmental changes in the Nile catchment area as inferred from Nile upper continental slope sediments. *Quaternary Science Reviews* 130, 200-221.

672 Said, R. (1993) *The River Nile: Geology, Hydrology and Utilization*, Oxford.
673 Sestini, G. (1989) Nile Delta: a review of depositional environments and geological history. In
674 M.G.K. Whateley, K.T. Picketing (Eds), *Deltas: Sites and Traps for Fossil Fuels, 99-127*.
675 Geol. Soc. London Spec. Publ., 41.
676 Shaltout, K.H., Khalil, M.T. (2005) *Lake Burullus: Burullus Protected Area*. Publication of
677 National Biodiversity Unit No. 13. EEAA/MedWetCoast Project, Cairo.
678 Shanahan, T.M., Mckay, N.P., Hughen, K.A., Overpeck, J.T., Otto-Bliesner, B., Heil, C.W., King,
679 J., Scholz, C.A., Peck, J. (2015) The time-transgressive termination of the African Humid
680 Period. *Nature Geoscience* 8(2), 140-144.
681 Sivan, D., Eliyahu, D., Raban, A. (2004) Late Pleistocene to Holocene Wetlands Now Covered
682 by Sand, along the Carmel Coast, Israel, and their Relation to Human Settlement: An
683 Example from Dor. *Journal of Coastal Research* 204, 1035-1048.
684 Stanley, J.D., Warne, A.G. (1997) Holocene sea level change and early human utilization of
685 deltas. *GSA Today* 7(12), 1-7.
686 Stanley, J.D., Chen, Z. (1991) Distinguishing sand facies in the Nile Delta, Egypt, by stained
687 grain and compositional component analyses. *Journal of Coastal Research* 7(3), 863-877.
688 Stanley, J.D., Warne, A.G. (1993) Nile Delta: Recent Geological Evolution and Human Impact.
689 *Science* 260, 628-634.
690 Stanley, J.D., Clemente, P.L. (2017) Increased land subsidence and sea level rise are
691 submerging Egypt's Nile Delta coastal margin. GSA Today 27(5), 4-11.
692 Stuiver, M., Reimer, P.J. (1993) Extended 14C database and revised CALIB radiocarbon
693 calibration program. Radiocarbon 35, 215-230.
694 Stuiver, M., Reimer, P.J., Reimer, R.W. (2020) CALIB 8.2 [WWW program] at http://calib.org,
695 accessed 2020-4-22.

696 Syvitski, J.P., Kettner, A.J., Overeem, I., Hutton, E.W., Hannon, M.T., Brakenridge, G.R., Day, J.,
697 Vörösmarty, C., Saito, Y., Giosan, L. Nicholls, R.J. (2009) Sinking deltas due to human
698 activities. *Nature Geoscience* 2(10), p.681.
699 Thompson, R., Oldfield, F. (1986) Environmental Magnetism. George Allen & Uniwin, London.
700 Tessler, Z.D., Vörösmarty, C.J., Grossberg, M., Gladkova, I. Aizenman, H. (2016) A global
701 empirical typology of anthropogenic drivers of environmental change in deltas.
702 *Sustainability science* 11(4), 525-537.
703 Tierney, J.E., Pausata, F.S.R., De Menocal, P.B. (2017) Rainfall regimes of the green Sahara.
704 *Science Advances* 3(1), e1601503.
705 Törnqvist, T.E. (1994) Middle and late Holocene avulsion history of the River Rhine (Rhine-
706 Meuse delta, Netherlands). *Geology* 22(8), 711-714.
707 Törnqvist, T.E., González, J.L., Newsom, L.A., van der Borg, K., de Jong, A.F.M., Kurnik, C. W.
708 (2004). Deciphering Holocene sea-level history on the U.S. Gulf Coast: A high-resolution
709 record from the Mississippi Delta. *GSA Bulletin*, 116 (7-8): 1026–1039.
710 Toussoun, O. (1922) *Mémoires Sur Les Anciennes Branches Du Nil, époque Ancienne.* Mémoire
711 de l'Institut d'Egypte 4, Le Caire.
712 UNDP/UNESCO (1978) *Coastal Protection Studies. Project Findings and Recommendations*.
713 Paris, UNDP/EGY/73/063, 483 pp.
714 Vacchi, M., Ghilardi, M., Melis, R. T., Spada, G., Giaime, M., Marriner, N., Lorscheid, T.,
715 Morhange, C., Burjachs, F., Rovere, A. (2018). New relative sea-level insights into the
716 isostatic history of the Western Mediterranean. *Quaternary Science Reviews* 201, 396-
717 408.
718 Warner, K., Erhart, C., de Sherbinin, A., Adamo, S.B., Chai-Onn, T.C. (2009) “In search of
719 Shelter: Mapping the effects of climate change on human migration and displacement.”

720 A policy paper prepared for the 2009 Climate Negotiations. Bonn, Germany: United
721 Nations University, CARE, and CIESIN-Columbia University and in close collaboration with
722 the European Commission “Environmental Change and Forced Migration Scenarios
723 Project”, the UNHCR, and the World Bank.
724 Wang, L.X., Brook, G.A., Burney, D.A., Voarintsoa, N.R.G., Liang, Y.L., Cheng, H., Edwards, L.
725 (2019) The African Humid Period, rapid climate change events, the timing of human
726 colonization, and megafaunal extinctions in Madagascar during the Holocene: Evidence
727 from a 2m Anjohibe Cave stalagmite. *Quaternary Science Reviews* 210, 136-153.
728 Welc, F., Marksb, L. (2014) Climate change at the end of the Old Kingdom in Egypt around
729 4200 BP: New geoarchaeological evidence. *Quaternary International* 324, 124-133.
730 Wilson, C.A. .Hughes, Z.J., FitzGerald, D.M., Kolker, A.S., Lynch, J.C., Rosen, P. (2020) Saltmarsh
731 sustainability throughout the Holocene in Boston Harbor: A new sea-level curve for the
732 lower Gulf of Maine and implications of recent anthropogenic alteration. *Quaternary*
733 *Science Reviews* 240, 106383.
734 Wilson, P. (2012) Waterways, settlements and shifting power in the north-western Nile Delta.
735 *Water History* 4, 95-117.
736 Wilson, P. (2018) Human and deltaic environments in northern Egypt in late antiquity. *Late*
737 *antique archaeology* 12(1), 42-62.
738 Wunderlich, J. (1988) Investigations on the development of the Western Nile Delta in
739 Holocene times. In: E.C.M. van den Brink (ed.) *The archaeology of the Nile Delta, Egypt:*
740 *problems and priorities*, 251-257. Amsterdam: Netherlands Foundation for
741 Archaeological Research in Egypt.

742 Zhao, X., Thomas, I., Salem, A., Alassal, S.E., Liu, Y., Sun, Q., Chen, J., Ma, F., Finlayson, B., Chen,
743 Z. (2020) Holocene climate change and its influence on early agriculture in the Nile Delta,
744 Egypt. *Palaeogeography, Palaeoclimatology, Palaeoecology* 547, 109702.
745 Zuo, X., Lu, H., Li, Z., Song, B., Xu, D., Zou, Y., Wang, C., Huan, X., He, K. (2016) Phytolith and
746 diatom evidence for rice exploitation and environmental changes during the early mid-
747 Holocene in the Yangtze Delta. *Quaternary Research* 86(3), 304-315.

748
749
750

751 **Figure and table captions**

752 **Figure 1:** The Nile Delta, showing: 1) Burullus Lagoon and sediment core site BR-1; 2) paleo-
753 coastline of ca. 7-5 ka (after Said, 1981); 3) paleo-Nile branches (Said, 1981), and 4)
754 sediment cores collected from previous studies (Core 1-2 from Sestini, 1989; S-cores from
755 Arbouille and Stanley, 1991). The basaltic distribution of the Blue Nile was after Revel et
756 al. (2010). Square in black shows the archaeological site of Buto (discussed in text).
757
758 **Figure 2:** AMS-^{14}C-dated Holocene sediment sequences of BR-1. The age-depth model was
759 reconstructed using the dedicated R-code Clam (Blaauw, 2010) and sedimentation rates
760 were calculated.
761
762 **Figure 3.** Reconstructed relative sea level of Burrulus coast, using both dated peat layers and
763 lagoon muds from this study and dated peat layers from Arbouille and Stanley (1991).4.2.
764 Bio-sedimentology of core BR-1
765
766 **Figure 4.** Distribution of sediment magnetic susceptibility (MS), TIC, TOC, macro-fauna and
767 ostracod of core BR-1. Our data were used to define nine sedimentary units (A-I). * - age
768 cited from Arbouille and Stanley (1991) and Chen and Stanley (1993)
769
770 **Figure 5.** Diagnostic geochemical elements (Al, Fe, Ti, Cr, Zr, Hf) and their normalized values
771 (to Al) of core BR-1 (data from the peat layers are not included). Magnetic susceptibility

(MS) is listed for comparison. * - age cited from Arbouille and Stanley (1991) and Chen and Stanley (1993).

Figure 6. Comparison of Fe/Al and Ti/Al of this study to $^{87}Sr/^{86}Sr$ of core S21 (Nile Delta) and water level proxy (δDWax ‰) of the Blue Nile basin

Figure 7. Holocene sediment core transect of Burullus lagoon-coast: A) along-coast; B) perpendicular to coast. Fluvial sediment facies prevail on the eastern lagoon coast, and marshland on the central-west lagoon coast. Holocene sediment core (1-2) and S-cores were collected from Sestini (1989); and Arbouille and Stanley (1991).

Figure 8. Sketch map, showing the Holocene evolution of Burullus lagoon

Table 1. Details of AMS-^{14}C-dating materials of BR-1. ^{14}C dates were expressed in calibrated years BP at the 95% confidence level (2σ). Accepted ^{14}C dates were used for Age-depth model.